Journal of Solid State Chemistry **168,** 76–84 (2002)
doi:10.1006/jssc.2002.9683

Low-Frequency Relaxation Phenomena in α-$LiIO_3$: The Nature and Role of Defects

Y. Mugnier,*[,1] C. Galez,* J. M. Crettez,† P. Bourson,‡ C. Opagiste,* and J. Bouillot*

*Laboratoire d'Instrumentation et de Matériaux d'Annecy, Université de Savoie, 5 chemin de Bellevue, Annecy le Vieux, BP806 74016 Annecy Cedex, France; †Laboratoire de Physique de l'Université de Bourgogne, CNRS UMR 5027, 9 Av. Alain Savary, BP47870, 21078 Dijon Cedex, France; and ‡Laboratoire Matériaux Optiques Photonique et Systèmes, Université de Metz CNRS FRE2304, CLOES-SUPELEC, 2 Rue E Belin, 57078 Metz Cedex, France

Received March 21, 2002; in revised form June 6, 2002; accepted June 17, 2002

The lithium iodate ionic conduction in the polar *c*-axis direction is studied between 35 and 470 K for crystals grown in various conditions. So far, to separate processes induced by the nature of electrodes, the impedance spectroscopy technique had been used at room temperature with both metallic and ideally polarizable insulating electrodes, so that a relaxation of space charges was clearly identified. Here, the temperature dependence of the hopping ionic conductivity exhibits quite different activation energies well related to the growth conditions. Following low-temperature Raman and thermodynamic experiments, a new approach based on a vacancy diffusion mechanism is proposed. Experimental conductivity results are then correlated with the valence, size and concentration of extrinsic impurities incorporated during the growth and analyzed by plasma spectroscopy. Finally, a discussion is made on still not well-understood phenomena such as the strong increase of photorefractivity or the enhancement of some Bragg reflections. © 2002 Elsevier Science (USA)

Key Words: **lithium iodate; ionic conductivity; extrinsic defects; growth conditions; chemical analyses; impedance spectroscopy.**

1. INTRODUCTION

Lithium iodate in its hexagonal structure (α-$LiIO_3$) is a polar non-ferroelectric material used for its large transparency range and excellent nonlinear optical properties. It could be also a new challenger in the field of frequency self-doubling materials or parametric amplifiers. From a fundamental aspect, the highly anisotropic ionic conductivity of α-$LiIO_3$ has been widely studied. Nevertheless, it appears that many discrepancies exist in the corresponding literature, which are due to the fact that experimental responses depend not only on intrinsic parameters such as acidity of the growth solution and doping, but also on external ones such as the amplitude of the electric field and the nature of the electrodes used in the experiments (1). Besides, some still not well-understood phenomena happen when submitting samples to a high dc electric field along the *c*-axis. Among them, the enhancement of some Bragg reflections has been intensively investigated by means of synchrotron radiation and conventional X ray or neutron diffraction experiments (2, 3). Another related phenomenon (4) is the formation of grating lines extending from the cathode to the anode when a static field (about a few $kV\,cm^{-1}$) is applied in the *c*-axis direction. A common feature in all these phenomena is the "freezing" of the effect when the sample is cooled down to 200–240 K and, in any case, the influence of the ionic conduction is suggested even if the mechanisms and the kind of charge carriers are not yet well identified.

In a previous work (5), the dielectric behavior of α-$LiIO_3$ in the polar *c*-axis direction had been investigated at room temperature, for crystals grown under different conditions, through impedance spectroscopy. First, it was shown that either rigid metal electrodes or (chemically inert) ideally polarizable insulating ones were required to obtain reliable results with this material. Then, it was observable that the low-frequency dielectric response was ruled out by the formation of a space charge zone. Finally, admittance diagrams were drawn which led to the determination of the true value of the hopping ionic conductivity corresponding to a macroscopic movement of ionic charges in phase with the applied electric field.

In the present work, the impedance spectroscopy technique is used to investigate the temperature dependence of ionic conductivity from 35 to 470 K for various crystals grown in different conditions (pH and doping of

[1] To whom correspondence should be addressed. Fax: +33-450-09-66-49. E-mail: yannick.mugnier@esia.univ-savoie.fr.

0022-4596/02 $35.00

the growth solution). The corresponding results are related to chemical analyses in order to establish the correlation between the hopping ionic conductivity and the impurities present in the samples. The good agreement obtained between the experimental data and the proposed microscopic approach together with low-temperature thermodynamic investigations seems to contradict the assumption of the existence of an ionic–superionic transition, which is usually suggested in literature for this material (6).

2. EXPERIMENTAL DETAILS

α-$LiIO_3$ single crystals were grown as described in a previous paper (7). Undoped crystals grown from neutral (pH = 6) or acid (pH = 2) supersaturated aqueous solutions and Cr^{3+}-doped ones were investigated in the *c*-axis direction with an HP4284A impedance analyser. Experiments were carried out by imposing an electric field with amplitude ranging from 10^{-2} to $10\,V\,cm^{-1}$ and frequency ranging from 20 Hz to 1 MHz, where no ac amplitude dependence of the measured capacitance is detectable.

Room temperature (RT) experiments were performed with the experimental setup detailed in (5) and a customized measurement cell, consisting of polished rigid copper films maintained with steel compression springs, was developed for temperature investigations. The edge capacitance has been reduced by using a guarded electrode and slow heating and cooling rates, which have been adjusted at $0.5\,K\,min^{-1}$.

Chemical analyses have been performed at the "Service Central d'Analyse" belonging to C.N.R.S. of France. Coupled plasma and mass spectroscopy yielded the amount of impurities with a resolution of 0.1 ppm in mass.

3. RESULTS

3.1. Chemical Analyses

Chemical analyses have been effected with three kinds of samples, each one originating from the same single crystal used for the corresponding dielectric measurements described below. The related results are given in Table 1 for samples grown with the following conditions:

(a) pH of the growth solution = 2, without deliberate impurities;
(b) pH of the growth solution = 2, with 0.01% (mol.) Cr^{3+};
(c) pH of the growth solution = 6, without deliberate impurities.

Detected impurities have been classified according to their valence and size (ionic radius for a coordination number of 6) (8). The total number of impurities is denoted n_{tot} expressing the sum of the number of the divalent (n_{di}) and trivalent (n_{tri}) defect ions. For the microscopic approach which will be detailed below, the notations n_1 and n_2 are also introduced in order to discriminate ionic species with radius close to 1 and to 0.7 Å, respectively.

TABLE 1
Plasma and Mass Spectroscopy Analyses Related to the Growth Conditions of α-$LiIO_3$ Crystals

Growth conditions	Element	Charge	Ionic radius (Å) [8]	Molar concentration (ppm)
(a) *Undoped* pH = 2 *crystal*				
(n_{tot} = 92 ppm)	Ce	3+	1.01	13
	La	3+	1.03	9
n_{tri} = 26 ppm	Nd	3+	0.98	4
n_{di} = 66 ppm	Sr	2+	1.18	6
	Mg	2+	0.72	52
n_1 = 32 ppm	Pt	2+	0.80	2
n_2 = 60 ppm	Mn	2+	0.83	6
(b) pH = 2 *crystal with* 0.01% (mol.) Cr^{3+}				
(n_{tot} = 305 ppm)	Cr	3+	0.62	175
	Al	3+	0.54	54
	Ce	3+	1.01	2
n_{tri} = 235 ppm	La	3+	1.03	4
n_{di} = 70 ppm	Mg	2+	0.72	60
n_1 = 11 ppm	Sr	2+	1.18	5
n_2 = 294 ppm	Mn	2+	0.83	5
Undoped pH = 6 *crystal*				
(n_{tot} = 48 ppm)	Cd	2+	0.95	1
n_{tri} = 2 ppm	Ti	3+	0.67	2
n_{di} = 46 ppm	Mg	2+	0.72	45

These analyses clearly reveal a strong dependence of the chemical composition on the growth conditions as it was expected since, in the literature, many experimental results devoted to α-$LiIO_3$ are not always consistent. Moreover, in the field of optical materials, growth of crystals with well-defined properties and controlled content of defects is today a challenging task. Such chemical analyses are thus of primary interest to adapt the growth conditions to a specific application (9).

3.2. RT Dielectric Response

Before going deeper in the temperature investigations, it is useful to briefly describe how the RT dielectric response is affected by the sample chemical composition. When rigid metal electrodes are used, the response of an undoped pH = 2 plate of thickness $e = 1.52$ mm is illustrated by the complex admittance diagram of Fig. 1 in which it is compared with that of a neutral-type crystal ($e = 1.03$ mm) and a chromium-doped one (0.05% mol, $e = 2.83$ mm, pH = 2).

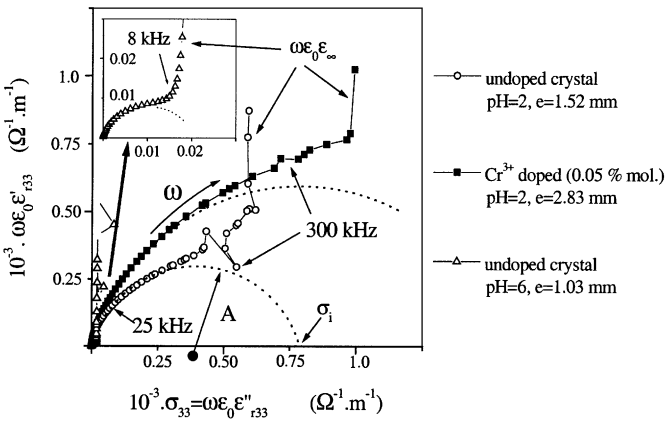

FIG. 1. RT admittance diagram for different α-$LiIO_3$ crystals.

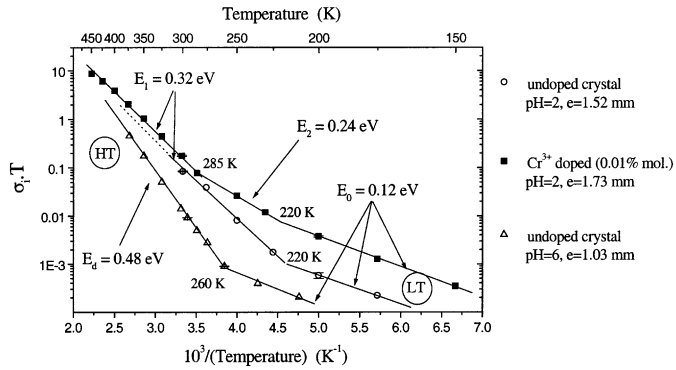

FIG. 3. Temperature dependence of the hopping ionic conductivity for different α-$LiIO_3$ crystals: *LT = low-temperature domain, *HT = high-temperature domain.

From an electrical point of view, this non-ideal dipolar response can be modelled by a series R–C circuit in parallel with a frequency-independent capacity C_∞ representing any physical process having a faster response. Since electrodes are blocking layers for the ionic charge carriers, the hopping ionic conductivity σ_i leading to the space charge accumulation is deduced from the high-frequency limit of the real part of admittance (represented in Fig. 1 by the slightly tilted dotted circle of radius A) (10). As the disturbances in the 300 kHz region should be attributed to the piezoelectricity of α-$LiIO_3$ (5), it results that the ionic conductivity of the Cr-doped sample ($\sigma_i = (1.70 \pm 0.02) \times 10^{-5}\,\Omega^{-1}\,cm^{-1}$) is nearly twice that of the undoped plate with pH = 2 ($\sigma_i = (0.80 \pm 0.02) \times 10^{-5}\,\Omega^{-1}\,cm^{-1}$). For the neutral-type crystal, the relaxation of space charges is shifted towards low frequencies and the smaller value of σ_i is measured equal to $(0.019 \pm 0.001) \times 10^{-5}\,\Omega^{-1}\,cm^{-1}$.

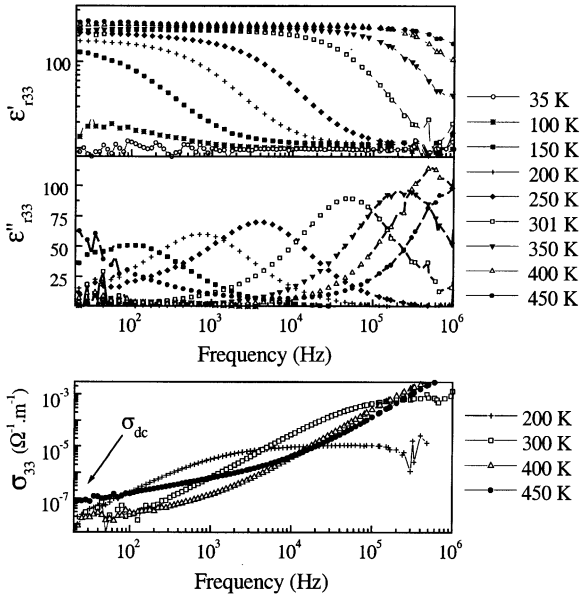

FIG. 2. Temperature dependence of ε'_{r33}, ε''_{r33} and σ_{33} for a Cr^{3+} doped (0.01% mol.) pH = 2 α-$LiIO_3$ crystal ($e = 1.73$ mm).

3.3. *Temperature Dependence of Relaxation Phenomena*

In order to identify mass and electrical transport in α-$LiIO_3$, i.e., the mechanism of ions diffusion and the type of charge carriers (predominant intrinsic or extrinsic defects) which are responsible for the RT relaxation of space charges, dielectric measurements have been performed in the range 35–470 K. Representative dielectric spectra, including the real (ε'_{r33}) and imaginary (ε''_{r33}) part of the permittivity are depicted in Fig. 2. For a Cr-doped sample, they show a shift of the relaxation peak towards high frequencies when temperature is raised. For lowest temperature, the high-frequency permittivity ε_∞ (i.e., free from accumulation of the space charges) becomes measurable and is found to be around 15. This value appears to present no temperature evolution as it is expected for ionic and electronic polarisabilities.

The corresponding temperature dependence of the ac conductivity σ_{33} is also presented in Fig. 2. Note that all spectra are characterized by a high-frequency plateau associated with the hopping ionic conductivity σ_i and that the low-frequency component σ_{dc} is observable, with our experimental setup, only for temperature higher than 400–450 K.

Afterwards, the bulk ionic conductivity σ_i, deduced either from the admittance diagram or relaxation frequency ω_0 ($= \sigma_i/\varepsilon_0\varepsilon'_{r33}$), is illustrated by Fig. 3, where the product $\sigma_i \cdot T$ is plotted in terms of $1/T$. For all samples, a strong dependence on the growth conditions appears since different activation energy domains and transition temperatures are observed. In the low-temperature (LT) region, the same slope ($E_0 = 0.12 \pm 0.01$ eV) is found for all crystals, but above 220 K (resp. 260 K), that is in the high-temperature (HT) domain, the activation energy

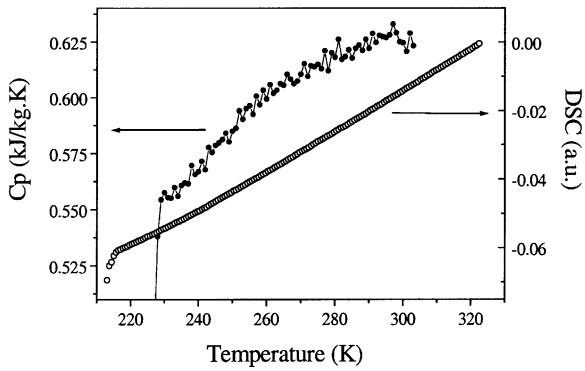

FIG. 4. DSC curve and temperature dependence of specific heat C_p for a pure acid (pH = 2) α-$LiIO_3$ crystal.

becomes $E_1 = 0.32 \pm 0.01$ eV (resp. $E_d = 0.48 \pm 0.01$ eV) for the acid (resp. neutral)-type undoped plates. For the Cr^{3+}-doped acid-type plate, the HT domain (above 285 K) presents an activation energy equal to E_1, but an additional domain is measured between 220 and 285 K for which $E_2 = 0.24 \pm 0.02$ eV.

It is worth mentioning that these results agree with many experimental studies (6, 11–14). However, the relatively weak values of the RT ionic conductivity together with the sequence of phase transitions (15–17) seem to contradict the existence of a second-order ionic–superionic transition which is often suggested in the relating literature to explain the activation energy change below RT. Such transitions usually occur near the melting point (≈ 703 K for α-$LiIO_3$) with a strong increase in entropy and a weak maximum of specific heat (18). Therefore, to go further in this topic, thermodynamic and Raman spectroscopy measurements have been done especially in the 200–300 K region.

3.4. Thermodynamic and Raman Spectroscopy Investigations

Thermodynamic investigations, experimentally studied with a DSC-7 *Perkin Elmer* calorimeter, are depicted in Fig. 4. The differential scanning calorimetry experiment made under argon and with a heating rate of 5 K min^{-1} exhibits no enthalpic peak meaning that there is no structural phase transition between 215 and 320 K. Moreover, the temperature dependence of specific heat C_p, follows roughly the same evolution as recently published data (19) even if, in our case, no special anomaly could be noticed between 230 and 303 K (here, the sharp rise below 225 K is attributed to the system thermal stabilization). The continuous evolution of specific heat would indicate the absence of a second-order phase transition.

With the aim of understanding the origins of the activation energy changes in the temperature dependence of σ_i, we have also performed Raman investigations below RT since the eventual ionic–superionic transition was associated with a cooperative or non-cooperative motion of Li^+ ions along *c*-axis (6). It can be seen in Fig. 5 that, on one hand, there is no first-order crystallographic transition between 30 and 483 K as it has been already pointed out in (15). On the other hand, a special attention is paid to the external symmetric A-type mode $\nu_2^A \approx 240\ cm^{-1}$, which has been previously attributed, thanks to a simple force-constant model, to translation of Li^+ ions along the *c*-axis (20). One can observe a decrease in the height of the peak as temperature increases, but the integrated intensity remains constant since the linewidth enlarges correspondingly. Therefore, no special feature could be detected corresponding to the occurrence of a superionic transition.

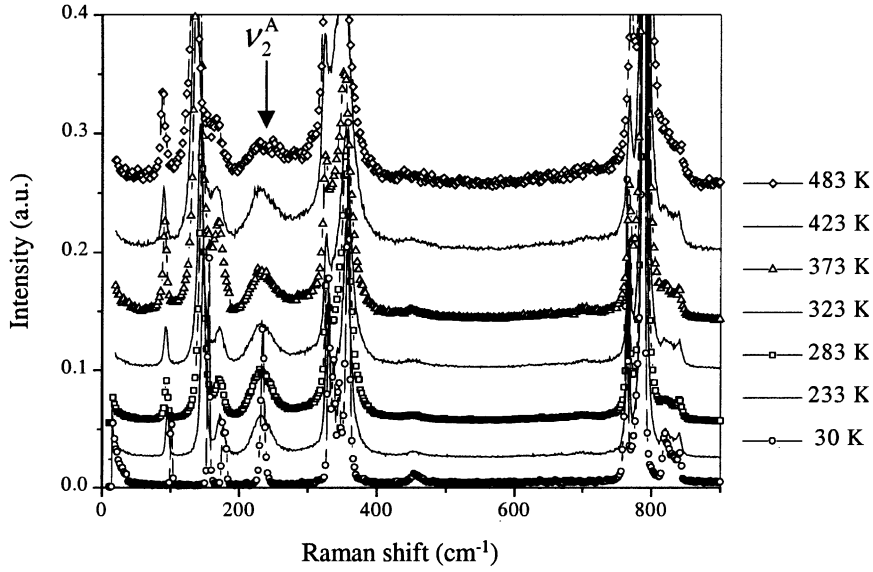

FIG. 5. Temperature dependence of the Raman A modes in the *y*(*zz*)*x* configuration for a Cr^{3+} doped (0.01% mol.) pH = 2 α-$LiIO_3$ crystal.

Besides, similar results were obtained by Cerdeira *et al.* (21) and show that the ν_2^A mode broadens considerably more than any of the other Raman-active modes, but this strong anharmonic effect does not appear in the range 200–300 K. In fact, the ν_2^A mode broadening was observed below 100 K which would indicate some relationships with the ionic conductivity, in this temperature range, and hence the existence of induced polarization effects. Such effects were indeed detected and studied thereafter by monitoring the temperature evolution of the low-frequency permittivity.

3.5. Evolution of the Low-Frequency Permittivity

The temperature dependence obtained for the low-frequency permittivity is reported in Fig. 6. For the variously grown crystals, the HT apparent permittivity $\varepsilon_{HT,A}$ observed above $\sim$250 K corresponds to the RT relaxation of space charges. As the measured capacity C ($= \varepsilon_0 \varepsilon'_{r33} S/e$) is independent on the sample thickness e, the real part of permittivity seems to vary linearly with e, leading to an apparent permittivity proportional to the sample thickness (5). Above RT and for a weak ac electric field, this low-frequency permittivity does not present any other special feature up to 450 K.

On the other hand, a kind of plateau, delimited in Fig. 6 by double-ended arrows, can be observed for each sample. It is quite important to note that the smaller the frequency is, the more visible and defined the plateau is. The low-temperature static permittivity $\varepsilon_{LT,S}$ ($+\varepsilon_\infty$) corresponding to the plateau height is indeed less clearly defined for the pH = 6 sample, for which the driven frequency was increased from 25 to 100 Hz. In fact, this new feature in the lithium iodate dielectric properties is no longer discernible above 1 kHz.

Hence, to summarize experimental results, both the low-frequency permittivity and the Arrhenius temperature dependence of ionic conductivity (i.e., activation energy domains and transition temperatures) are strongly related to the growth conditions, which greatly affect the sample composition and, consequently, the amount of defects. Thus, the next section deals with a new microscopic approach based on a vacancy diffusion mechanism and allowing us to correlate the experimental responses with the valence, size and concentrations of extrinsic impurities.

4. MICROSCOPIC APPROACH

Belonging to the space group $P6_3$, α-lithium iodate possesses a channelling structure responsible for the diffusion processes and corresponding polarization effects are only observable along the *c*-axis. In this direction, the superposition of joined oxygen octahedra containing Li^+ ions results in a quasi-one-dimensional ionic conductivity (15–17).

Many EPR studies carried out on $LiIO_3$ doped with metal and rare ions in divalent or trivalent state conclude that doping ions replace Li^+ ones, the charge compensation being ensured by, respectively, one or two lithium vacancies in the nearest site along z (22–26). For chromium-doped crystals, Zheng and Wu (27) recently proposed a mechanism where a temperature increase dissociates defects formed by one Cr^{3+} ion and the two associated Li^+ vacancies with the following reaction:

$$(V'_{Li} - Cr^{\bullet\bullet}_{Li} - V'_{Li})^x \rightarrow (V'_{Li} - Cr^{\bullet\bullet}_{Li})^{\bullet} + V'_{Li}$$

written here under the standard Kröger notation. Lithium vacancies are then nearly free to move in the structural channels and interact with both Li^+ ions and/or impurity-associated defects. This latter case being less probable,

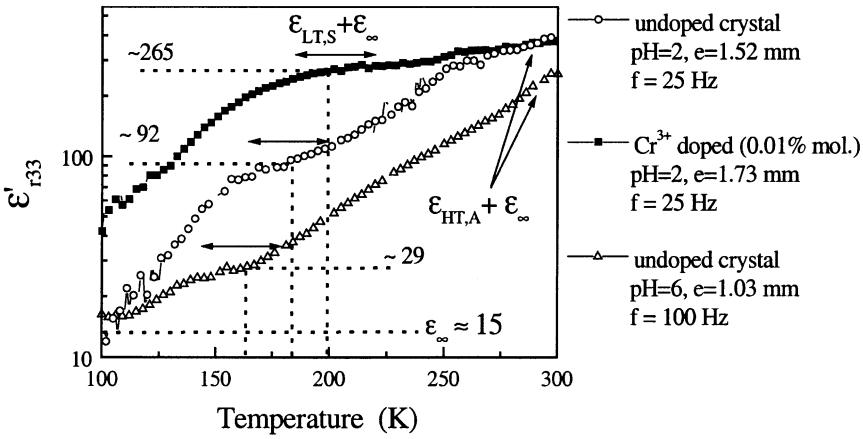

FIG. 6. Temperature dependence of low-frequency permittivity for different α-$LiIO_3$ crystals.

owing to the small number of defects, it seems reasonable to attribute the common LT domain E_0 (Fig. 3) to lithium ions hopping (according to a vacancy mechanism) between higher potential barriers due to the extrinsic impurities. From an energetic point of view, jumps of impurities in a close vacant site should be less probable than lithium ones and, since dissociation of the defects associated with divalent impurities are electrostatically less favorable than for trivalent ones, we can consider that the LT domain comes from migration of vacancies dissociated from trivalent impurities. The resulting migration of vacancies and the induced polarization effects should depend only on the number of free moving vacancies (i.e., the concentration of trivalent impurities corresponding to n_{tri} in Table 1) and the total concentration of defects ($n_{tot} = n_{tri} + n_{di}$) partially blocking the channels. At low temperature this polarization corresponds to $\varepsilon_{LT,S}$ as it is shown below.

4.1. Derivation of the Low-Temperature Static Permittivity $\varepsilon_{LT,S}$

Considering a set of oscillating charges q in a symmetric double-well potential, corresponding to two sites i and j separated by a distance d (d stands here for $c/2 \approx 2.58$ Å with c the cell parameter along the c-axis) and assumed to be temperature independent, the application of a parallel static or low-frequency electric field modifies direct and reverse jump rates. It results in the appearance of a dipolar Debye-like polarization for which the induced static permittivity (called here $\varepsilon_{LT,S}$) becomes, in a one-dimensional description, (10, p. 33):

$$\varepsilon_{LT,S} = \varepsilon'_{r33} - \varepsilon_\infty = Np\frac{qd}{kT\varepsilon_0} f_i f_j, \qquad [1]$$

where ε_0 is the permittivity of vacuum, k the Boltzmann constant, N the volume number of identical non-interacting dipole moments p and f_i, f_j the time-averaged probabilities of occupation for sites i and j (which are close to $\frac{1}{2}$ in the case of N identical double wells). For hopping charges, the dipole moment p physically corresponds to a distance–charge product. Thus, in the case of a homogeneous and uniform distribution of impurities partially blocking the displacements of nearly free vacancies, the dipole moment due to the long-range migration is

$$p = qd\frac{n_{Li}}{n_{tot}}, \qquad [2]$$

where n_{Li} ($\approx 1.50 \times 10^{28}$ at. m^{-3}) represents the total number of Li^+ ions and dn_{Li}/n_{tot} the mean distance between impurities. Combination of Eqs. [1] and [2] leads to the relationship

$$\varepsilon_{LT,S} = n_{tri}\frac{n_{Li}}{n_{tot}}\frac{q^2d^2}{4kT\varepsilon_0} = \frac{n_{tri}}{n_{tri}+n_{di}}\frac{n_{Li}q^2d^2}{4kT\varepsilon_0}, \qquad [3]$$

TABLE 2
Comparison between Experimental and Calculated Values of the Low Temperature Static Permittivity $\varepsilon_{LT,S}$ of α-$LiIO_3$ Crystals

Sample	n_{tri} (ppm)	n_{tot} (ppm)	T (K)	$(\varepsilon'_{r33} - \varepsilon_\infty)_{exp} = \varepsilon_{LT,S}$	$(\varepsilon_{LT,S})_{cal}$
Undoped pH = 2 crystal	26	92	185	$(92-15) \approx 77$	80
Cr^{3+}-doped 0.01%, pH = 2	235	305	200	$(265-15) \approx 250$	201
Undoped pH = 6 crystal	2	48	165	$(29-15) \approx 14$	15

where the classical one-dimensional static permittivity is multiplied by a ratio taking into account both divalent and trivalent impurities. In Table 2, the results of the chemical analyses are used to calculate this induced static permittivity corresponding to a "dipole length relaxation."

In spite of experimental errors (as in the thermal stabilization of the sample or in the precision of chemical analyses) and the assumption of a uniform distribution of impurities, a relatively good agreement is obtained, for all the crystals, between calculated values and experimental data deduced from Fig. 6. This confirms that the dissociation of defects associated with trivalent impurities is the predominant LT mechanism. It also gives rise to a vacancy diffusion process with the weak activation energy $E_0 = 0.12$ eV between potential barrier of extrinsic defects and, thus, to the (bulk) LT dipolar relaxation. Finally, when frequency is increased, this relaxation also accounts for the plateau disappearing observed in Fig. 6 since above ~ 1 kHz vacancies have no more enough time to accumulate at the blocking defects before the ac electric field is reversed.

4.2. Low- and High-Temperature Diffusion Mechanisms

4.2.1. Acid-type crystals. As the RT dielectric response is associated with a relaxation of space charges and the LT domain with migration of vacancies between defects, we may assume that activation energies E_1 and E_2 are related to the jumps of thermally activated impurities into vacant sites. In this way, for acid-type crystals, the higher activation energies E_1 and E_2 of Fig. 3 would be related to the size of impurity ions since two groups of ionic radii, respectively, n_1 (~ 1 Å) and n_2 (~ 0.7 Å), appear in Table 1. Interactions of vacancies with lithium and impurity ions are then described following the simple and commonly used symmetric linear hopping model.

In the case of a periodic one-dimensional potential, the effective jump rate for lithium ions becomes, in the weak

field approximation (18, 28):

$$v_{\mathrm{Li}} = v_0 \frac{qEd}{kT} \exp\left(\frac{-E_0}{kT}\right), \quad [4]$$

where v_0 is the attempt frequency ($\approx 7 \times 10^{12}$ Hz, corresponding to the Raman v_2^{A} mode), E the external applied electric field, E_0 ($=0.12$ eV) the LT activation energy and d (≈ 2.58 Å) the jump distance. If we still assume a uniform distribution of impurities, the mean distance between impurity ions of the same size can be written dn_{Li}/n_1 and dn_{Li}/n_2 so that we may define the following two new effective jump rates corresponding to the jumps of impurities into vacant sites:

$$v_1 = v_0 \frac{n_{\mathrm{Li}}}{n_1} \frac{qEd}{kT} \exp\left(\frac{-E_1}{kT}\right), v_2 = v_0 \frac{n_{\mathrm{Li}}}{n_2} \frac{qEd}{kT} \exp\left(\frac{-E_2}{kT}\right), \quad [5]$$

where E_1 ($=0.32$ eV) and E_2 ($=0.24$ eV) correspond to the experimental HT activation energies. In this way, a direct comparison between v_{Li}, v_1 or v_2 (each one being associated with one activation energy) allows to determine the transition temperature between the different domains of Fig. 3 as follows:

— For the undoped pH = 2 crystal with predominant domains E_0 and E_1, chemical analyses yield $n_1 = 32$ ppm, so that the transition temperature derived from $v_{\mathrm{Li}} = v_1$ becomes:

$$T = \frac{(E_1 - E_0)}{k \ln(n_{\mathrm{Li}}/n_1)} = \frac{(0.32 - 0.12) \times 1.6 \times 10^{-19}}{1.38 \times 10^{-23} \ln(10^6/32)} = 224\ \mathrm{K} \quad [6]$$

which is in quite good agreement with the experimental value of ~ 220 K determined in Fig. 3. Interactions of vacancies with large ionic radius impurities thus define the HT mechanism of activation energy E_1. It results in a macroscopic diffusion of vacancies, actually responsible for the space charge accumulation.

— Considering the Cr^{3+}-doped acid-type crystal, the jumps of thermally activated impurities also regulate the HT migration of vacancies. Comparison between v_1 and v_2 with the impurity concentrations n_1 ($=11$ ppm) and n_2 (294 ppm) gives the transition temperature equal to

$$T = \frac{(E_1 - E_2)}{k \ln(n_2/n_1)} = 282\ \mathrm{K} \quad [7]$$

which is still comparable with the experimental value of 285 K. However, the comparison between v_2 and v_{Li} leads to a transition temperature of 172 K, i.e., below the experimental change from E_0 to E_2 observed at 220 K. This discrepancy may be explained by the presence of larger concentrations of impurities with lower jump rates and also by the small extent of the temperature region defining the intermediate domain (i.e., the accuracy for the determination of E_2). For example, in the case of Fe^{3+} (ionic radius ≈ 0.55 Å) doped acid-type crystals Xu *et al.* (13) determined, in the range 193–300 K, an activation energy of 0.26 ± 0.02 eV with which we obtain a transition temperature of $T = 200 \pm 28$ K consistent with Fig. 3.

So, to conclude about the mechanisms and nature of charge carriers in the case of acid-type crystals, we can say that the above microscopic approach based on a comparison of effective jump rates accounts for the present experimental responses and also for those appearing in various published articles since content of defects in α-$LiIO_3$ is rarely specified. This large diffusion of vacancies dissociated from defects associated with trivalent impurities has indeed the merit to correlate the growth conditions or sample chemical composition with the activation energies and transition temperatures currently observed.

Moreover, it is worth noting that the above approach considers that an ideal homogeneous distribution of impurities exists. This assumption, already mentioned as an error source on the $\varepsilon_{\mathrm{LT,S}}$ derivation, could also explain the non-ideal Debye response in both LT and HT domains. Linear fits of $\varepsilon''_{\mathrm{r}33}$ below and above the relaxation frequency give absolute slopes named m and $(n-1)$ in Refs. (5, 10), lying in the range 0.4–0.8 which are commonly found in ionic conductive materials. In solid electrolytes, this dielectric peak broadening is either related to a cooperative motion of interacting ions or to a distribution of relaxation times induced by the different potential barriers of non-equivalent crystallographic sites (29). Here, both the HT space charge accumulation and the LT diffusion of vacancies between randomly distributed defects imply different diffusion lengths. As a consequence, a distribution of diffusion times is expected, which corresponds to the observed non-ideal dipolar relaxation that is simultaneously affected by the sample composition and temperature of investigation.

4.2.2. Neutral-type crystals. According to chemical analyses, the neutral-type crystal greatly differs from the acid ones in the sense that the major part of incorporated impurities is divalent. Trivalent metallic ions such as Cr^{3+} or Al^{3+} ions found in acid-type crystals behave, in aqueous solution, as Lewis acids thus forming polynuclear complexes in neutral or basic environment (30, 31). These complexes certainly prevent the incorporation of the corresponding ions during the crystal growth.

It results that the higher HT activation energy $E_d = 0.48$ eV showed by neutral crystals is no more related to the vacancies dissociated from trivalent impurities, but from divalent ones (Mg^{2+} or Cd^{2+}). Indeed, the association enthalpy of defects, including two effective

monovalent charges q_i and q_j separated by a distance d in a medium of permittivity ε_∞ (≈ 15), is given by the simple relation (32):

$$E_d = \frac{q_i q_j}{4\pi\varepsilon_0\varepsilon_\infty d} = 0.37\,\text{eV}. \qquad [8]$$

As the LT activation energy E_0 is associated with hopping of lithium ions, the HT domain for neutral samples comes from the following dissociation reaction of defects associated with divalent impurities:

$$(Mg^{\bullet}_{Li} - V'_{Li})^x \rightarrow Mg^{\bullet}_{Li} + V'_{Li}$$

for which the experimental slope of 0.48 eV is the sum of a diffusion enthalpy term ($E_0 = 0.12$ eV) and a dissociation one (0.37 eV).

4.3. *Ionic Conductivity and Specific LT Lithium Iodate Properties*

In previous sections, it has been shown that the growth-dependent ionic conductive properties of lithium iodate crystals are well determined by the vacancies dissociated from impurity defects. Now, as conductive materials are characterized by long-range migration of charge carriers and polarization by finite displacements (10) it appears that both neutral- and acid-type crystals are relevant of these two physical properties. The LT domain indeed behaves as a "dielectric state" where the blocked diffusion of vacancies gives raise to a bulk dipole-length relaxation phenomenon. Then, according to sample composition, increasing temperature around 220–260 K activates impurity jumps to form the HT ionic conductive state where long-range displacements of vacancies participate to the space charge accumulation.

The transition temperature range between these two states also coincides with the "freezing" effect of some Bragg reflections enhancement and the formation of grating lines extending from the cathode to the anode when a static electric field is applied in the c-axis direction (2–4). As mentioned in introduction, these not well-understood phenomena were related to a decrease of the ionic conduction even if the mechanisms and charge carriers were not clearly identified. From our point of view, these features are now better explained by the present microscopic approach. Lowering temperature changes the long-range redistribution of vacancies to a bulk one and then, prevents the formation of space charges partially responsible for the above phenomena (33, 34). According to the sample composition, this frozen LT redistribution could also account for the appearance of a strong photorefractive effect below 200–220 K where small displacements of vacancies stop screening the photoinduced electronic charge-density grating during two-wave mixing experiments (12, 13).

Finally, let us recall that the transition between LT and HT domains was also highlighted by monitoring the temperature dependence of longitudinal acoustic waves absorption. Below RT, the maximum absorption was found to greatly depend on the growth conditions (6, 13). This latter fact, usually attributed to an intrinsic cooperative motion of Li^+ ions, seems to be governed, more likely, by the behavior of extrinsic defects. The same conclusion can be drawn from experimental studies of the polar lithium iodate properties. The long-range migration of vacancies can be induced by spontaneous polarization since temperature dependence of the pyroelectric coefficient shows a minimum at 200–220 K (resp. 250 K) for acid- (resp. neutral) type crystals (35–37), i.e., in agreement with the ionic conductivity evolution of Fig. 3 leading to the HT space charge accumulation.

5. CONCLUDING REMARKS

Once the concentration of impurities being precisely determined by coupled plasma and mass spectroscopy, the lithium iodate ionic conductive properties were investigated between 35 and 450 K for crystals grown in various conditions. The results show that both diffusion enthalpies or activation energies and temperatures of transition between LT and HT domains are strongly dependent on the growth conditions. This strong dependence seems to exclude the existence of an intrinsic second-order ionic–superionic transition as it has been confirmed by LT thermodynamic and RAMAN experiments. This is also relevant to the proposed microscopic approach that allows us to correlate the experimental responses with the valence, size and concentrations of extrinsic defects. In the case of acid-type crystals, the assumption of a diffusion mechanism of vacancies is consistent with the high amount of trivalent incorporated impurities resulting in the HT activation energies well related to the size of impurities. For neutral samples, chemical analyses yield a major concentration of divalent impurities for which the vacancy-impurity association enthalpy or electrostatic interaction well accounts for the experimental activation energy still associated with a vacancy mechanism.

In our opinion, the most important feature lies in the bulk-to-long range displacements of vacancies defining the transition between the LT "dielectric state"—the accumulation of vacancies at the blocking extrinsic defects was proved by simple calculations on the induced static permittivity—and the HT conductive domain. Increasing temperature, therefore, leads to the formation of space charges. This whole redistribution of vacancies actually affects the pyroelectric coefficient, the strength of the

photorefractive effect and the reduction or extinction of some Bragg reflections.

ACKNOWLEDGMENTS

The authors would like to thank Prof. Gachon (University of Nancy, France) for making possible the low-temperature thermodynamic investigations. M. Maglione (ICMC Bordeaux, France) is also gratefully acknowledged for fruitful discussions.

REFERENCES

1. A. A. Blistanov, N. S. Koslova, and V. V. Geras'kin, *Ferroelectrics* **198,** 61 (1997).
2. J. Bouillot, J. Baruchel, M. Remoissenet, J. Joffrin, and Lajzerowicz, *J. Phys.* **43,** 1259 (1982).
3. Y. Li, *Adv. Sci. Chin. Phys.* **1,** 45 (1985).
4. J. Baruchel, J. Bouillot, and E. Coquet, *Philos. Mag. B* **63,** 1051 (1991).
5. Y. Mugnier, C. Galez, J. M. Crettez, P. Bourson, and J. Bouillot, *Solid State Commun.* **115,** 619 (2000).
6. A. E. Aliev, A. Sh. Akramov, L. N. Fershtat, and P. K. Khabibullaev, *Phys. Stat. Sol. A* **108,** 189 (1988).
7. C. Galez, C. Rosso, Y. Teisseyre, J. M. Crettez, P. Bourson, G. Medeiros-Ribeiro, A. Righi, and R. L. Moreira, *Solid State Commun.* **93,** 1013 (1995).
8. D. R. Lide, "Handbook of Chemistry and Physics," CRC Press, Boca Raton, FL, 2001.
9. V. Grachev and G. Malovichko, *Phys. Rev. B* **62,** 7779 (2000).
10. A. K. Jonscher, "Dielectric Relaxation in Solids," Chelsea Dielectric Press Ltd., London, 1983.
11. V. V. Vorob'ev, A. A. Kuleshov, E. V. Charnaya, A. A. Abramovich, S. V. Alchangyan, B. I. Kydiarov, and M. N. Kul'bitskaya, *Sov. Phys. Solid State* **31,** 1670 (1989).
12. J. Xu, X. Yue, and R. A. Rupp, *Phys. Rev. B* **54,** 16618 (1996).
13. J. Xu, H. Kabelka, R. A. Rupp, F. Laeri, and U. Vietze, *Phys. Rev. B* **57,** 9581 (1998).
14. L. G. Jacobsohn, P. Lunkenheimer, F. Laeri, U. Vietze, and A. Loidl, *Phys. Stat. Sol. B* **198,** 871 (1996).
15. J. M. Crettez, E. Coquet, B. Michaux, J. Pannetier, J. Bouillot, P. Orlans, A. Nonat, and J. C. Mutin, *Physica B* **144,** 277 (1987).
16. M. Czank, H. Schulz, and H. G. Wiedeman, *Z. Kristallogr.* **143,** 99 (1976).
17. J. K. Liang, G. H. Rao, and Y. M. Zhang, *Phys. Rev. B* **39,** 459 (1989).
18. C. Deportes, M. Duclot, P. Fabry, J. Fouletier, A. Hammou, M. Kleitz, E. Siebert, and L. Souquet, "Electrochimie des Solids," Presses Universitaires de Grenoble, Grenoble, 1994.
19. N. R. Abdulchalikova, A. E. Aliev, V. F. Krivorotov, and P. K. Khabibullaev, *Sol. State Ionics* **107,** 59 (1998).
20. J. M. Crettez, J. P. Misset, and E. Coquet, *Solid State Commun.* **34,** 297 (1980).
21. F. Cerdeira, F. E. A. Melo, and V. Lemos, *Phys. Rev. B* **27,** 7716 (1983).
22. M. Krupski, A. A. Mirzakhanyan, W. Hilczer, and E. G. Sharoyan, *Phys. Stat. Sol. B* **133,** 355 (1986).
23. W. C. Zheng, *Phys. Stat. Sol. B* **153,** K103 (1989).
24. D. M. Daraseliya and D. L. Japaridze, *Phys. Stat. Sol. B* **119,** K57 (1983).
25. D. L. Dzaparidze, S. V. Alchyangyan, D. M. Daraseliya, and T. I. Sanadze, *Sov. Phys. Solid State* **31,** 502 (1989).
26. W. C. Zheng and S. Y. Wu, *Physica B* **271,** 252 (1999).
27. W. C. Zheng and S. Y. Wu, *J. Phys.: Condens. Matter* **11,** 3127 (1999).
28. J. C. Dyre, *Phys. Rev. B* **49,** 11709 (1994).
29. F. Henn, J. Vanderschueren, J. C. Giuntini, and J. V. Zanchetta, *J. Appl. Phys.* **85,** 2821 (1999).
30. H. B. Gray and G. P. Haight, "Principles de Chimie," InterEditions, Paris, 1982.
31. P. Barnum, *Inorg. Chem.* **22,** 2300 (1983).
32. Y. T. Chiang, D. Birnie, and W. D. Kingery, "Physical Ceramics. Principles for Ceramic Science and Engineering," John Wiley & Sons Inc., New York, 1997.
33. S. J. Gu and Y. Y. Li, *Chin. Phys.* **4,** 260 (1984).
34. G. Zhang, J. Liu, and S. Feng, *Chin. Phys. Lett.* **2,** 83 (1985).
35. J. Del Cerro, S. Ramos, F. Jimenez, and J. M. Sanchez-Laulhe, *Ferroelectrics* **54,** 187 (1984).
36. R. Poprawski, J. Shaldon, and S. Matyjasik, *Phys. Stat. Sol. A* **90,** 167 (1985).
37. A. S. Bhalla, *J. Appl. Phys.* **55,** 1229 (1984).